Typeset using jjap.cls <ver.1.0.1>

Correlation between the inner electric field and the photocurrent of Zn-phthalocyanine Schottky-barrier cells

Ichiro Hiromitsu* and Genki Kinugawa

Department of Material Science, Faculty of Science and Engineering
Shimane University, Matsue 690-8504

(Received)

Electroabsorption(EA) study with an electric-field modulation frequency $\omega_m/(2\pi)$ of 1 Hz is carried out for two types of typical organic Schottky-barrier cells, Au/Zn-phthalocyanine (ZnPc)/Al and Au/ZnPc/In/Al, in order to elucidate the role of the inner electric field in the photocurrent ($I_{\rm photo}$) generation. From the bias dependence of the 1F- and 2F-EA intensities measured at the frequencies of ω_m and $2\omega_m$, respectively, it is shown that the inner electric field E_0 as well as the modulation electric field E_m is quenched in the ZnPc layer with the forward bias larger than $\sim$1 V. For Au/ZnPc/Al, a good correlation is observed between E_0 and $I_{\rm photo}$, which indicates that $I_{\rm photo}$ is generated by E_0. For Au/ZnPc/In/Al, on the other hand, no correlation is observed between E_0 and $I_{\rm photo}$. An interpretation of the latter is that $I_{\rm photo}$ is caused by an increase of the charge-injection probability at the ZnPc/In interface as a result of the trapping of photogenerated charges in the interface region. For both systems, the depletion layer is detected by a capacitance-voltage measurement at 0.2 Hz.

KEYWORDS: solar cells, Schottky barrier, organic semiconductors, phthalocyanine, electroabsorption, admittance

*E-mail address: hiromitu@riko.shimane-u.ac.jp

1. Introduction

The organic-thin-film solar cells have been studied as the candidates for the practical devices based on organic semiconductors.[1,2] However, the mechanism of the photocurrent generation in the organic solar cells is not yet clearly understood. The mechanism should be closely related to the distribution of the inner electric field in the device because the inner electric field may cause the dissociation of the excitons as well as the drift of the electrons and holes. This is the reason why the study of the inner electric field has a critical importance.

The inner electric field is usually studied by electroabsorption (EA) spectroscopy,[3–5] in which an electric-field modulation is applied to the device and a synchronous change in the optical-absorption coefficient is detected. The 1F-EA signal intensity, which is the EA intensity detected at the fundamental modulation frequency ω_m, is proportional to $E_0 E_m$, where E_0 is the inner electric field and E_m is the modulation electric field. Usually, E_m is assumed to be constant in the organic layers. Then, the 1F-EA intensity becomes simply proportional to E_0. Recently, we have studied the correlation between E_0 and the photocurrent of Zn-phthalocyanine (ZnPc)/perylene derivative (PTCBI) heterojunction solar cells in order to elucidate the role of E_0 in the generation of photoexcited carriers.[6] A good correlation was observed between E_0 and the photocurrent for the ZnPc layer indicating that the excitons are dissociated by E_0, while, for the PTCBI layer, an anomalous electric field was detected in the interface region which did not have any correlation with the photocurrent.

In the present paper, an EA study is carried out for two types of typical Schottky-barrier cells, Au/ZnPc/Al and Au/ZnPc/In/Al. By measuring the 2F-EA intensity, which is the EA intensity detected at the frequency of $2\omega_m$, it will be shown that the modulation electric field E_m is not constant in the ZnPc layer, which indicates that the 1F-EA intensity is not simply proportional to the inner electric field E_0. It will be shown, however, that the information about E_0 still can be obtained. We have already reported an EA study for Au/ZnPc/Al, in which the features of the insulating layer at the ZnPc/Al interface was discussed.[7] In this previous study, however, only the 1F-EA measurement

with the modulation frequency of 100 Hz was carried out for a very limited bias range. In the present study, a much more comprehensive study will be carried out with the measurements of the 1F- and 2F-EA intensities for a wider bias range with the modulation frequency of 1 Hz as well as the measurements of the dark current, admittance and photocurrent. As a result, the bias dependence of the inner electric field E_0 and the role of E_0 in the photocurrent generation will be elucidated.

2. Experiment

2.1 Sample preparation

ZnPc was purchased from Kanto Chem. Co. Inc. and was used after subliming three times in vacuum. Au of 99.95 % purity, Al and In of 99.99 % were purchased from Nilaco Corp.

Two types of ZnPc Schottky-junction systems, i.e. Au/ZnPc/Al and Au/ZnPc/In/Al were prepared as shown in Fig. 1. On a quartz substrate of $9 \times 24 \times 1$ mm^3, the thin films were evaporated under a pressure of 1×10^{-4} Pa. The Al film in Au/ZnPc/In/Al is a supporting electrode for In because the electric conductivity of the In film is quite poor.[8] The film thickness was 13 nm for Au, 100 nm for ZnPc, 20 nm for In and 25 nm for Al. The speed of the evaporation was 0.02 nm/s for Au, 0.1 nm/s for ZnPc and Al, and 0.01 nm/s for In, monitored by a quartz oscillator (ULVAC CRTM5000 or CRTM6000). The active area of the device measures 0.3 cm^2. All the measurements were carried out with the sample in the air at room temperature.

2.2 Admittance measurement

The circuit for the admittance measurement is shown in Fig. 2. The parallel connection of the conductance G_p and capacitance C_p in Fig. 2 is an equivalent circuit for the sample. A sinusoidal input voltage $V_{\rm in} = V_0 \sin\omega t$ with a frequency $\omega/(2\pi)$ between 0.2 and 10^5 Hz and an amplitude V_0 of 0.05 V was applied to the circuit, and the output signal $V_{\rm out} = AV_0 \sin(\omega t + \delta)$ across a small resistance r was observed using a digital oscilloscope. Then, the conductance G_p and the capacitance C_p were obtained from the gain A and the phase shift δ.[9] The value of the resistance r was chosen to be between 1 kΩ and 100 kΩ depending on the frequency and the applied bias voltage so as to be sufficiently low

compared to the impedance of the sample.

2.3 EA measurement

The inner electric field was studied by the electroabsorption (EA) measurement, in which an electric-field modulation $E_m \sin\omega_m t$ was applied to the device and a synchronous change in the optical-absorption coefficient was detected. The change, $\Delta\alpha$, in the optical-absorption coefficient has the following relationship with the static inner electric field E_0 in the device:[6]

$$\Delta\alpha \propto \mathrm{Im}\chi^{(3)} \left\{ \left(E_0^2 + \frac{E_m^2}{2} \right) + 2E_0 E_m \sin\omega_m t - \frac{E_m^2}{2} \cos 2\omega_m t \right\}, \tag{1}$$

where $\mathrm{Im}\chi^{(3)}$ is the imaginary part of the third-order electric susceptibility. Equation (1) indicates that the amplitude of the response in the fundamental frequency ω_m is proportional to $E_0 E_m$, while that of the $2\omega_m$ response is proportional to E_m^2.

The electric circuit for the EA measurement is shown in Fig. 1. An electric-field modulation was applied to the sample by using a function generator whose output signal was $V_m \sin\omega_m t$ with a modulation frequency $\omega_m/(2\pi)$ of 1 Hz and an amplitude V_m of 0.5 or 0.25 V. The probe light was entered normally to the active area of the device from the quartz side. The light source was a 100 W halogen lamp followed by a monochromator. The light intensity depended on the wavelength but was always smaller than 20 μW/cm^2. The transmitted light intensity T was detected by a photomultiplier tube. The change, ΔT, of the transmitted light intensity due to the electric-field modulation was measured by using a lock-in amplifier. ΔT is related to the change, $\Delta\alpha$, of the optical-absorption coefficient of ZnPc by the following equation:

$$-\frac{\Delta T}{T} = d \times \Delta\alpha, \tag{2}$$

where d is the depth of the ZnPc layer into which the modulation electric field is effectively applied.

2.4 Photocurrent measurement

Two types of photocurrent measurements were carried out. One is the measurement of the stationary-state photocurrent which was detected by a lock-in amplifier under

an illumination of a 630-nm light chopped at 10 Hz. The light source for this type of measurement was the same as that for the EA measurement, and the illumination was from the quartz side. The positive directions of the photocurrent and the applied bias voltage are defined in Fig. 1(a).

The other type of the measurement is for the time dependence of the photocurrent after turning on and off the light. For this type of measurement, a 633-nm light of 600 μW/cm^2 was used which was obtained by using a He-Ne laser of 5 mW and a beam expander. The illumination was from the quartz side. The switching time for turning on and off the light was 50 μs. The transient signal was accumulated and averaged by using a digital oscilloscope.

3. Results

3.1 Dark J-V characteristics

Figure 3 shows the bias dependence of the dark current density of the Au/ZnPc/Al and Au/ZnPc/In/Al cells. The rectification ratio at $V_{\rm bias} = \pm 2$ V is 30.6 for Au/ZnPc/Al and 1050 for Au/ZnPc/In/Al. The current density of Au/ZnPc/Al is smaller than that of Au/ZnPc/In/Al by more than two orders of magnitude. This suggests that an insulating layer exists at the ZnPc/Al interface.

3.2 Admittance

Figure 4 shows the frequency dependence of the conductance G_p and capacitance C_p of Au/ZnPc/Al and Au/ZnPc/In/Al under the bias voltage $V_{\rm bias}$ of $+2$, 0 and -2 V. Generally, G_p is determined by the sum of two contributions, i.e. the conductivity due to free carriers and the dielectric relaxation of localized charges, while C_p is determined only by the latter. The former contribution G_0 due to free carriers corresponds to the low-frequency limit of G_p since the contribution from the dielectric relaxation disappears in this limit.[9] As seen in Fig. 4(a), G_0 becomes larger by applying the forward bias, which is directly related to the rectification properties shown in Fig. 3. In the whole frequency range between 10^{-1} and 10^5 Hz, G_p decreases and C_p increases as the frequency is lowered. Since C_p in the frequency range between 10^4 and 10^5 Hz does not have significant bias dependence, the frequency dependence of C_p and G_p in this frequency

range is not related to the localized charges because the number of the localized charges should be bias dependent, but is attributed to the intrinsic response rate of the present systems: Consider that the present system is equivalent to an RC circuit connected in series, having a response rate of $1/(RC)$. The conductance $g_p(\omega)$ and capacitance $c_p(\omega)$ of this RC circuit become,

$$g_p(\omega) = \frac{(\omega CR)^2}{R[1+(\omega CR)^2]}, \tag{3a}$$

$$c_p(\omega) = \frac{C}{1+(\omega CR)^2}. \tag{3b}$$

These equations indicate that $g_p(\omega)$ decreases and $c_p(\omega)$ increases by decreasing the frequency near $\omega = 1/(RC)$. The frequency dependence of G_p and C_p in the range between 10^4 and 10^5 Hz in Fig. 4 is attributed to this type of frequency dependence. The similar frequency dependence has been reported for a C_{60} Schottky-barrier system.[9] The frequency dependence of G_p and C_p in the range between 10^{-1} and 10^4 Hz in Fig. 4, on the other hand, has a significant bias dependence, and is attributed to the dielectric relaxation of localized charges through their hopping motion.[9] The dielectric relaxation rate of the localized charges is distributed in a wide frequency range between 10^{-1} and 10^4 Hz.

In order to elucidate the features of the band bending in the system, the $1/C_p^2$-$V_{\rm bias}$ curves are plotted in Fig. 5 for the frequency of 0.2 Hz. This frequency was chosen because C_p has a significant frequency dependence for the higher frequencies. At 0.2 Hz, the localized charges can follow the applied alternating electric field so that the charge distribution in the systems is always in equilibrium. In Fig. 5, $1/C_p^2$ has a linear dependence on $V_{\rm bias}$ in the range of -0.8 V $\leq V_{\rm bias} \leq 0.4$ V for Au/ZnPc/Al and -1 V $\leq V_{\rm bias} \leq 0$ V for Au/ZnPc/In/Al.

The linear dependence is attributed to the dependence of the depletion-layer width on $V_{\rm bias}$. Due to the standard theory of the depletion capacitance,[10] the linear dependence of $1/C_p^2$ is formulated as follows.

$$\frac{1}{C_p^2} = \frac{2}{S^2 e\epsilon_0 \epsilon N_{\rm A}}(V_{\rm D} - V_{\rm bias}), \tag{4}$$

where $V_{\rm D}$ is the diffusion potential, $N_{\rm A}$ is the density of the negative localized charges in

the depletion layer, $S = 3.0\times10^{-5}$ m^2 is the effective area of the device, $\epsilon_0 = 8.85\times10^{-12}$ F/m is the permittivity of the free space and ϵ is the dielectric constant of ZnPc. ϵ is estimated to be 4.1 using the relationship $C = \epsilon\epsilon_0 S/d$, where $d = 1.0 \times 10^{-7}$ m is the film thickness of ZnPc and $C = 1.1 \times 10^{-8}$ F is the intrinsic capacitance of the present samples estimated from the value of C_p at 10^4 Hz for $V_{\rm bias} = 0$ V in Fig. 4. At this frequency, the localized charges do not respond to the alternating electric field, so that C_p is determined simply by ϵ, d and S of ZnPc with no contribution from the localized charges.

It is noted that Saleh et al. reported a value of ϵ as low as 1.56 for ZnPc films, which was estimated by a capacitance measurement at 1 kHz.[11] However, 1 kHz is obviously much higher than the response rate of their samples because they report a steep increase of C_p by lowering the frequency in the 100 Hz region for $V_{\rm bias} = 0$ V, indicating that the response rate is in the order of 100 Hz. The slow response rate is probably due to a large resistance of their samples which is larger by three orders compared to our samples. The measurement of the intrinsic capacitance C for the estimation of ϵ must be done at a lower frequency than the response rate of the system, as is seen from eq. (3b).

The straight lines in Fig. 5 are the calculated results using eq. (4). By this fitting, it is estimated that $V_{\rm D} = 0.50$ V and $N_{\rm A} = 2.1 \times 10^{23}$ m^{-3} for Au/ZnPc/Al and $V_{\rm D} = 0.24$ V and $N_{\rm A} = 1.5 \times 10^{23}$ m^{-3} for Au/ZnPc/In/Al. Then, the depletion-layer width W for $V_{\rm bias} = 0$ V is estimated to be 33 nm for Au/ZnPc/Al and 27 nm for Au/ZnPc/In/Al using the following relationship.[10]

$$W = \left\{ \frac{2\epsilon_0\epsilon(V_{\rm D} - V_{\rm bias})}{eN_{\rm D}} \right\}^{1/2}. \tag{5}$$

For Au/ZnPc/In/Al, $1/C_p^2$ in the range of 0 V$<$ $V_{\rm bias}$ $<$0.2 V deviates from the theoretical straight line. This is due to a significant increase in the number of localized charges as a result of the efficient injection under the forward bias condition.

3.3 Electroabsorption

Figure 6 shows the 1F-EA spectrum of Au/ZnPc/Al for $V_{\rm bias} = -2$ V detected at the fundamental modulation frequency ω_m. This spectrum is assigned to the ZnPc spectrum since it is in the same wavelength range with the optical absorption spectrum of ZnPc.[6] The similar EA spectrum with the identical line shape was observed also for

Au/ZnPc/In/Al. The EA-signal intensity $V_{\rm EA}$ is defined in Fig. 6 by the difference between the peak heights at 630 and 670 nm. Figure 7 shows the bias dependence of 1F-$V_{\rm EA}$ of Au/ZnPc/Al and Au/ZnPc/In/Al. At $V_{\rm bias} = 0$ V, 1F-$V_{\rm EA}$ has negative finite values, indicating that there exists a finite inner electric field E_0 in the ZnPc layer, because 1F-$V_{\rm EA}$ is proportional to $E_0 E_m$, where E_m is the modulation electric field. By increasing the reverse bias $V_{\rm bias} < 0$ V, the absolute value of 1F-$V_{\rm EA}$ increases. By increasing the forward bias $V_{\rm bias} > 0$ V, on the other hand, the absolute value of 1F-$V_{\rm EA}$ decreases and becomes nearly zero at $V_{\rm bias} \gtrsim 1$ V for Au/ZnPc/Al and $V_{\rm bias} \gtrsim 0.5$ V for Au/ZnPc/In/Al.

The 2F-EA spectrum of the present systems, detected at the frequency of $2\omega_m$, has the identical line shape with the 1F-EA spectrum shown in Fig. 6. Figure 8 shows the bias dependence of the 2F-EA intensity (2F-$V_{\rm EA}$). For both Au/ZnPc/Al and Au/ZnPc/In/Al, 2F-$V_{\rm EA}$ decreases by applying the bias of either sign. The decrease is steeper for the forward bias, and 2F-$V_{\rm EA}$ disappears at $V_{\rm bias} \gtrsim 1.5$ V for Au/ZnPc/Al and $V_{\rm bias} \gtrsim 0.8$ V for Au/ZnPc/In/Al. It is noted that no spectral broadening occurs by applying the bias, so that the decrease of the 2F-EA intensity really occurs. This result indicates that the modulation electric field E_m supplied to the ZnPc layer is bias dependent, because 2F-$V_{\rm EA}$ is proportional to E_m^2. The origin of the bias dependence of E_m will be discussed in §4.1

3.4 Photocurrent

Figure 9 shows the bias dependence of the photocurrent density $J_{\rm photo}$ of Au/ZnPc/Al and Au/ZnPc/In/Al, detected by a lock-in amplifier under an illumination of a 630-nm light chopped at 10 Hz from the Au side. The light source was the same as that for the EA measurement. In the case of Au/ZnPc/Al, the absolute value of $J_{\rm photo}$ increases by increasing the reverse bias, while, by increasing the forward bias, the absolute value of $J_{\rm photo}$ decreases and, for $V_{\rm bias} \gtrsim 1$ V, no photocurrent is observed. In the case of Au/ZnPc/In/Al, on the other hand, $J_{\rm photo}$ increases steeply in the forward bias region. Thus, the two systems have totally different $J_{\rm photo}$-$V_{\rm bias}$ characteristics.

Figure 10 shows the time dependence of $J_{\rm photo}$ of Au/ZnPc/Al after turning on and off a 633-nm light from a He-Ne laser. For $V_{\rm bias} = +2$ V (Fig. 10(a)), no photocurrent is detected in agreement with the result in Fig. 9(a). For $V_{\rm bias} = 0$ V (Fig. 10(b)), $J_{\rm photo}$

decreases steeply after turning on the light to a minimum value within 2 ms, and then, increases gradually to a negative equilibrium value with a time constant T_c of ~20 ms. After turning off the light, $J_{\rm photo}$ increases steeply to a maximum value within 2 ms, and then, gradually decreases to zero with $T_c \sim 20$ ms. For $V_{\rm bias}= -2$ V (Fig. 10(c)), the behavior after turning on the light is similar to that for $V_{\rm bias} = 0$ V, but T_c to reach the equilibrium value is ~600 ms which is much longer than that for $V_{\rm bias} = 0$ V. After turning off the light, $J_{\rm photo}$ increases steeply to zero within 2 ms.

Figure 11 shows the time dependence of $J_{\rm photo}$ of Au/ZnPc/In/Al. For $V_{\rm bias} = 0$ V (Fig. 11(b)), the features of the time dependence are similar to those for Au/ZnPc/Al, with the initial rise time after turning on and off the light being 0.2 ms, and T_c to reach the equilibrium values being ~3 ms. For $V_{\rm bias} = +2$ and -2 V (Figs. 11(a) and 11(c)), however, the features are totally different: $J_{\rm photo}$ reaches the equilibrium values monotonically after turning on and off the light. Thus, Au/ZnPc/Al and Au/ZnPc/In/Al have different photocurrent transients. A detailed discussion on the results of the photocurrent measurements will be given in §4.2.

4. Discussion

4.1 Inner Electric Field

When the EA technique is used to measure the inner electric field E_0 of the devices, the 1F-EA intensity (1F-$V_{\rm EA}$), which is proportional to E_0E_m, is usually measured on the assumption that the externally applied modulation electric field E_m is constant.[3–6] However, the strong bias dependence of the 2F-EA intensity (2F-$V_{\rm EA}$) in the present results in Fig. 8 indicates that E_m strongly depends on $V_{\rm bias}$ since 2F-$V_{\rm EA}$ is proportional to E_m^2.

The bias dependence of 2F-$V_{\rm EA}$ in the present results is interpreted separately for $V_{\rm bias} \lesssim 0$ V and $V_{\rm bias} > 0$ V. For $V_{\rm bias} \lesssim 0$ V, the bias dependence of 2F-$V_{\rm EA}$ is attributed to the bias dependence of the depletion-layer width as follows: The present modulation frequency of 1 Hz is sufficiently low so that the localized charges can follow the alternating electric field to keep the charge distribution in equilibrium at each moment. In this case, the modulation voltage $V_m \sin\omega_m t$ is supplied only to the depletion layer of width W, and

E_m in the depletion layer becomes V_m/W. As a result, only the depletion layer contributes to the EA signal, and 2F-$V_{\rm EA}$ should have the following relationship.

$$\text{2F-}V_{\rm EA} \propto E_m^2 W = \frac{V_m^2}{W} \propto \frac{V_m^2}{\sqrt{V_{\rm D} - V_{\rm bias}}}, \tag{6}$$

where eq. (5) was used for W. The calculated curves of eq. (6) using the value of $V_{\rm D}$ obtained by the present capacitance-voltage measurement in §3.2 are shown in Fig. 8. It is seen that the bias dependence of 2F-$V_{\rm EA}$ in the $V_{\rm bias} \lesssim 0$ V region is qualitatively explained by eq. (6). 1F-$V_{\rm EA}$, on the other hand, has the following relationship.

$$\text{1F-}V_{\rm EA} \propto E_d E_m W = E_d V_m, \tag{7}$$

where E_d is the inner electric field *in the depletion layer*. Thus, 1F-$V_{\rm EA}$ is proportional to E_d for $V_{\rm bias} \lesssim 0$ V. Since $E_d \sim (V_{\rm D} - V_{\rm bias})/W \propto \sqrt{V_{\rm D} - V_{\rm bias}}$, 1F-$V_{\rm EA}$ is expected to be proportional to $\sqrt{V_{\rm D} - V_{\rm bias}}$. The calculated curves for 1F-$V_{\rm EA}$ are shown in Fig. 7. The agreement between the experiment and the theory is satisfactory for $V_{\rm bias} \lesssim 0$ V.

For $V_{\rm bias} > 0$ V, the situation is totally different. The depletion layer width W becomes negligibly small, so that, if eq. (6) holds, 2F-$V_{\rm EA}$ is expected to increase by increasing $V_{\rm bias}$. However, the experimental value of 2F-$V_{\rm EA}$ decreases and disappears for $V_{\rm bias} \gtrsim 1$ V. This indicates that E_m becomes zero for $V_{\rm bias} \gtrsim 1$ V although a finite modulation voltage $V_m \sin \omega_m t$ is applied to the samples. In other words, the alternating modulation voltage does not affect the electric field in the ZnPc layer for $V_{\rm bias} \gtrsim 1$ V. Since the present modulation frequency of 1 Hz is so slow, the alternating modulation voltage and the slowly scanned DC bias voltage should have a similar effect: The scanning of the DC bias voltage for $V_{\rm bias} \gtrsim 1$ V should not affect the inner electric field E_0. Thus, E_0 should be constant for $V_{\rm bias} \gtrsim 1$ V. This constant value of E_0 should be zero because the experimental value of [1F-$V_{\rm EA}$]/$\sqrt{\text{[2F-}V_{\rm EA}\text{]}}$, which is proportional to E_0, becomes zero in the $V_{\rm bias} \sim 1$ V region. Thus, it is concluded that both E_0 and E_m are quenched in the ZnPc layer for $V_{\rm bias} \gtrsim 1$ V.

The quenching of E_0 and E_m may occur when the applied voltages $V_{\rm bias}$ and V_m are wasted at some part of the device. The location where this anomaly occurs is at the Au/ZnPc interface because of the following experimental observation: Three

types of samples having symmetric metal electrodes, Au/ZnPc/Au, Al/ZnPc/Al and Al/In/ZnPc/In/Al, were prepared, and their 1F-$V_{\rm EA}$ and 2F-$V_{\rm EA}$ were measured for -2 V $\leq V_{\rm bias} \leq 2$ V. Both 1F-$V_{\rm EA}$ and 2F-$V_{\rm EA}$ were zero for Au/ZnPc/Au in the whole bias range, while finite 1F-$V_{\rm EA}$ and 2F-$V_{\rm EA}$ were detected for Al/ZnPc/Al and Al/In/ZnPc/In/Al. This indicates that E_0 and E_m in the ZnPc layer is quenched for Au/ZnPc/Au by some sort of slipping of the Fermi level of Au relative to that of ZnPc at the Au/ZnPc interface. This slipping occurs only when a positive bias is applied to Au relative to ZnPc because, in the case of the Schottky junctions Au/ZnPc/Al and Au/ZnPc/In/Al, the anomaly occurs only under the forward bias condition. A more detailed study is in progress on the mechanism of this slipping. The band diagram deduced from the present results is shown in Fig. 12.

In our previous EA study of Au/ZnPc/Al,[7] the bias dependence of the 1F-EA intensity for 0 V $\leqq V_{\rm bias} \leqq +1$ V was explained by a model in which the effect of the insulating layer at the ZnPc/Al interface was taken into account. The present results indicate that the bias dependence of the EA intensity is strongly affected by the slipping of the Fermi levels at the Au/ZnPc interface. A correct model should take the effect of this slipping into account as well as the effect of the insulating layer, which is not possible at this moment because the features of the slipping have not been well understood.

4.2 Photocurrent

As shown in Fig. 9(a), the photocurrent density $J_{\rm photo}$ of Au/ZnPc/Al disappears for $V_{\rm bias} \gtrsim 1$ V. Since the inner electric field E_0 is also quenched in this bias region, $J_{\rm photo}$ has a good correlation with E_0. This indicates that the photoinduced carriers in Au/ZnPc/Al are generated and drifted by E_0. In the case of Au/ZnPc/In/Al, on the other hand, $J_{\rm photo}$ increases steeply for $V_{\rm bias} > 0$ V, having no correlation with E_0. The difference in the bias dependence of $J_{\rm photo}$ between the two systems may be related to the difference in the time dependence of $J_{\rm photo}$ in Figs. 10 and 11. Now, the mechanism of the time dependence is discussed.

The transient curves of Au/ZnPc/Al with $V_{\rm bias} = 0$ and -2 V (Figs. 10(b) and 10(c)) and of Au/ZnPc/In/Al with $V_{\rm bias} = 0$ V (Fig. 11(b)) are explained by an overlap of two

components:

$$J_{\text{photo}}(t) = f(t) + J_0, \tag{8}$$

where $f(t)$ is a capacitive component with a steep initial rise followed by a monotonic decay to zero and J_0 is a constant which expresses the stationary photocurrent density after turning on and off the light. The simulated curves for $f(t)$ and J_0 are shown in Figs. 10(b), 10(c) and 11(b). The value of J_0 is finite after turning on the light and zero after turning off, as expected. J_0 after turning on the light corresponds to the increase of the number of free carriers.

The capacitive component $f(t)$ originates from a sudden change of the charge distribution in the samples after turning on and off the light. By turning on the light, photoexcited carriers are generated, and some of them are trapped in the ZnPc layer. The negative and positive trapped charges distribute asymmetrically in the ZnPc layer because of the inner electric field. In order to compensate the voltage change by these trapped charges, electric current is induced through the external circuit, which corresponds to the component $f(t)$ after turning on the light. Similarly, $f(t)$ after turning off the light is an induced current due to a sudden disappearance of some of the trapped charges. In the case of $V_{\text{bias}} = -2$ V for Au/ZnPc/Al in Fig. 10(c), no capacitive component is seen after turning off the light. This is because the detrapping of the trapped charges occurs only very slowly, so that the induced current is negligibly small. This interpretation is supported by an experimental result shown in Fig. 13 in which the peak height ΔJ of the capacitive component $f(t)$ after turning on the light is plotted as a function of the period T_{dark} during which the light is kept off in the on-off cycles. The peak height ΔJ increases as T_{dark} increases, and does not reach the stationary value even for $T_{\text{dark}} = 160$ s. For the short T_{dark}, the light is turned on before all the trapped charges disappear, so that the increase of the number of the trapped charges by turning on the light is limited.

The time dependence of J_{photo} for Au/ZnPc/In/Al with $V_{\text{bias}} = \pm 2$ V in Figs. 11(a) and 11(c) has totally different features from the other cases. No capacitive component $f(t)$ is observed, and the time constant to reach the equilibrium value is in the order of $0.1 \sim 1$ s. The relatively long time constant indicates that the photocurrent involves a

trapping process. Since the photocurrent in these cases does not have a correlation with the inner electric field, the increase of the photocurrent is not attributed to the increase of the carrier density due to the dissociation of the excitons by the electric field. A possible interpretation may be that a small number of photogenerated charges are trapped near the ZnPc/In interface, which may affect the energy-barrier structure at the interface to enhance the charge-injection probability.[12)]

5. Conclusions

The admittance measurement of Au/ZnPc/Al and Au/ZnPc/In/Al showed that there exist free carriers and localized charges in the system, and the localized charges have a dielectric relaxation rate distributed between 10^{-1} and 10^{4} Hz, which originates from the hopping motion of the localized charges. Because of the slow dielectric relaxation, the observation of the depletion layer by the C-V measurement was possible with the frequency of 0.2 Hz.

The inner electric field was studied by the 1F- and 2F-EA measurements. An important finding is that the 2F-EA intensity has a strong bias dependence, which indicates that the modulation electric field E_m in the ZnPc layer is bias dependent although the applied modulation voltage V_m is constant. For $V_{\rm bias} < 0$ V, the bias dependence of the 2F- as well as the 1F-EA intensity is explained qualitatively by the usual theory of the depletion layer width eq. (5). For $V_{\rm bias} > 0$ V, on the other hand, both 1F- and 2F-EA intensities clearly deviates from the above theory, and the modulation electric field E_m and the inner electric field E_0 disappear in the ZnPc layer for $V_{\rm bias} \gtrsim 1$ V.

The photocurrent of Au/ZnPc/Al has a good correlation with the inner electric field E_0. This indicates that the photoexcited carriers in Au/ZnPc/Al are generated and drifted by E_0. For Au/ZnPc/In/Al, on the other hand, no correlation is observed between the photocurrent and E_0. The photocurrent transients of Au/ZnPc/Al and Au/ZnPc/In/Al have different features. It is interpreted that the photocurrent of Au/ZnPc/In/Al under the bias is generated by the change of the charge-injection probability at the ZnPc/In interface caused by the trapping of the photogenerated charges.

References

1) C. J. Brabec, N. S. Sariciftci, J. C. Hummelen: Adv. Funct. Mater. **11** (2001) 15.

2) H. Spanggaard and F. C. Krebs: Sol. Energy Mater. Sol. Cells **83** (2004) 125.

3) I. H. Campbell and D. L. Smith: *Conjugated Polymer and Molecular Interfaces*, eds. W. R. Salaneck, K. Seki, A. Kahn, J.-J. Pireaux (Marcel Dekker, New York, 2002) Chap. 21.

4) I. H. Campbell and M. D. Joswick: Appl. Phys. Lett. **67** (1995) 3171.

5) P. A. Lane, J. Rostalski, C. Giebeler, S. J. Martin, D. D. C. Bradley and D. Meissner: Sol. Energy Mater. Sol. Cells **63** (2000) 3.

6) I. Hiromitsu, Y. Murakami and T. Ito: J. Appl. Phys. **94** (2003) 2434.

7) I. Hiromitsu, Y. Murakami and T. Ito: Solid State Commun. **119** (2001) 357.

8) F.-R. Fan and L. R. Faulkner: J. Chem. Phys. **69** (1978) 3334.

9) I. Hiromitsu, R. Shinto, M. Kitano, T. Kitauchi and T. Ito: Jpn. J. Appl. Phys., Part 1, **41** (2002) 6517.

10) S. M. Sze: *Physics of Semiconductor Devices* (Wiley, New York, 1981) 2nd ed., Chap. 5.

11) A. M. Saleh, A. O. Abu-Hilal, R. D. Gould: Curr. Appl. Phys. **3** (2003) 345.

12) M. Hiramoto, S. Kawase and M. Yokoyama: Jpn. J. Appl. Phys., Part 2, **35** (1996) L349.

Figure captions

Fig. 1. Scheme of (a) Au/ZnPc/Al and (b) Au/ZnPc/In/Al and the electric circuit for the EA measurement.

Fig. 2. Electric circuit used for the admittance measurement. The parallel connection of the conductance G_p and capacitance C_p is an equivalent circuit for the sample.

Fig. 3. The bias dependence of the dark current density of (a) Au/ZnPc/Al and (b) Au/ZnPc/In/Al.

Fig. 4. The frequency dependence of (a) conductance G_p and (b) capacitance C_p of Au/ZnPc/Al (▲, ●, ▼) and Au/ZnPc/In/Al (△, ○, ▽). $V_{\rm bias} = +2$ V (▲, △), 0 V (●, ○), and -2 V (▼, ▽).

Fig. 5. The bias dependence of 1/[capacitance]^2 for (a) Au/ZnPc/Al and (b) Au/ZnPc/In/Al measured at 0.2 Hz. The solid lines are the calculated results using eq. (4).

Fig. 6. The 1F-EA spectrum of Au/ZnPc/Al with $V_{\rm bias} = -2$ V. The frequency $\omega_m/(2\pi)$ and the amplitude V_m of the electric field modulation $V_m \sin\omega_m t$ are 1 Hz and 0.5 V, respectively. The EA signal intensity $V_{\rm EA}$ is defined in the figure.

Fig. 7. The bias dependence of the 1F-EA intensity of Au/ZnPc/Al (●) and Au/ZnPc/In/Al (○). The frequency $\omega_m/(2\pi)$ and the amplitude V_m of the electric field modulation $V_m \sin\omega_m t$ are 1 Hz and 0.25 V, respectively. The broken curves are proportional to $\sqrt{V_{\rm D} - V_{\rm bias}}$ with $V_{\rm D} = 0.50$ V for Au/ZnPc/Al and 0.24 V for Au/ZnPc/In/Al.

Fig. 8. The bias dependence of the 2F-EA intensity of Au/ZnPc/Al (•) and Au/ZnPc/In/Al (○). The frequency $\omega_m/(2\pi)$ and the amplitude V_m of the electric field modulation $V_m \sin\omega_m t$ are 1 Hz and 0.50 V, respectively. The broken curves are proportional to $1/\sqrt{V_{\rm D} - V_{\rm bias}}$ with $V_{\rm D} = 0.50$ V for Au/ZnPc/Al and 0.24 V for Au/ZnPc/In/Al.

Fig. 9. The bias dependence of the photocurrent density of (a) Au/ZnPc/Al and (b) Au/ZnPc/In/Al by an illumination of a 630-nm light of 20 μW/cm^2 from the Au side.

Fig. 10. The time dependence of the photocurrent density of Au/ZnPc/Al with (a) $V_{\rm bias} = +2$ V, (b) 0 V and (c) -2 V after turning on and off a 633-nm light of 600 μW/cm^2. The broken lines for (b) and (c) represent the two components $f(t)$ and J_0 in eq. (8).

Fig. 11. The time dependence of the photocurrent density of Au/ZnPc/In/Al with (a) $V_{\rm bias} = +2$ V, (b) 0 V and (c) -2 V after turning on and off a 633-nm light of 600 μW/cm^2. The broken lines for (b) represent the two components $f(t)$ and J_0 in eq. (8).

Fig. 12. The band diagram for Au/ZnPc/In/Al deduced from the present results. Au/ZnPc/Al also has the similar band structure except that there exists an insulating layer at the ZnPc/Al interface.

Fig. 13. The peak height ΔJ of the capacitive component $f(t)$ of Au/ZnPc/Al after turning on the light vs. the period $T_{\rm dark}$ during which the light is kept off. $V_{\rm bias} = -2$ V. The illumination is with a 633-nm light of 600 μW/cm^2.

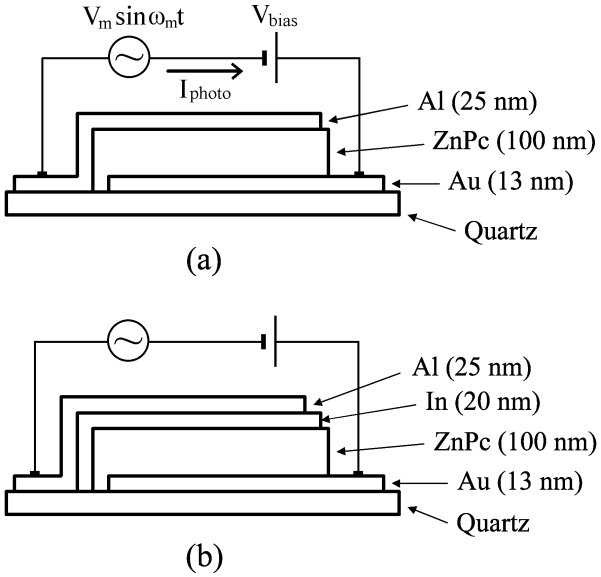

Fig.1 I. Hiromitsu et al.

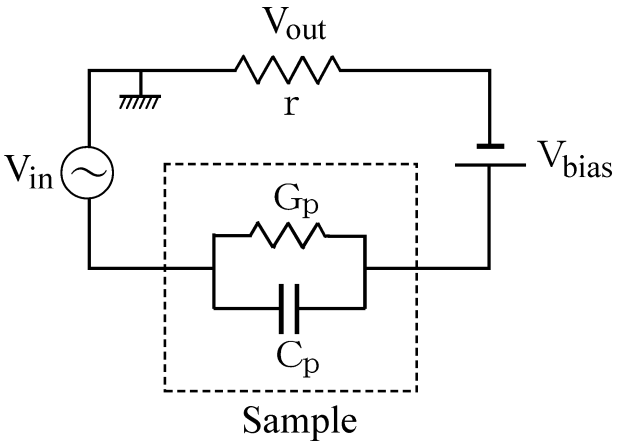

Fig.2 I. Hiromitsu et al.

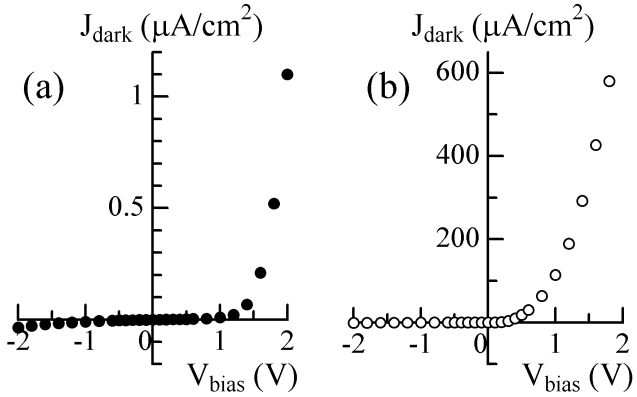

Fig.3 I. Hiromitsu et al.

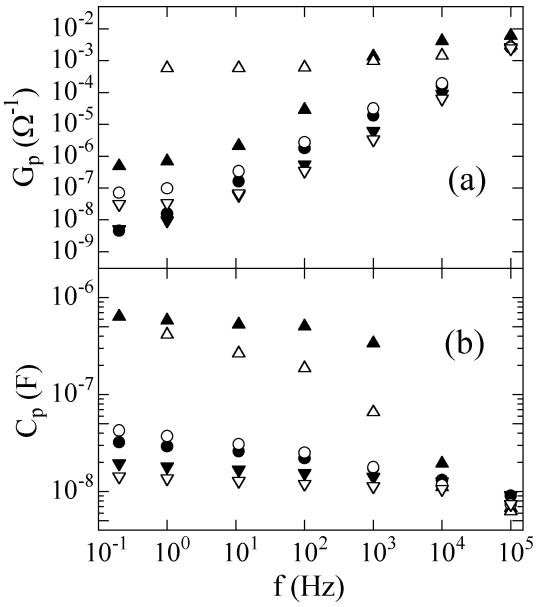

Fig.4 I. Hiromitsu et al.

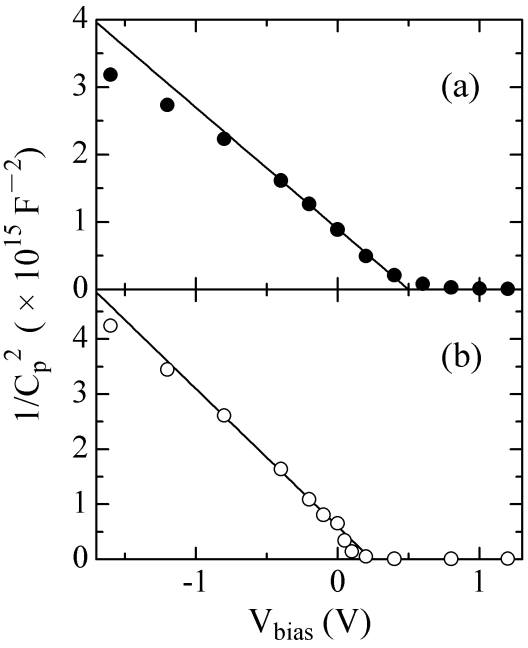

Fig.5 I. Hiromitsu et al.

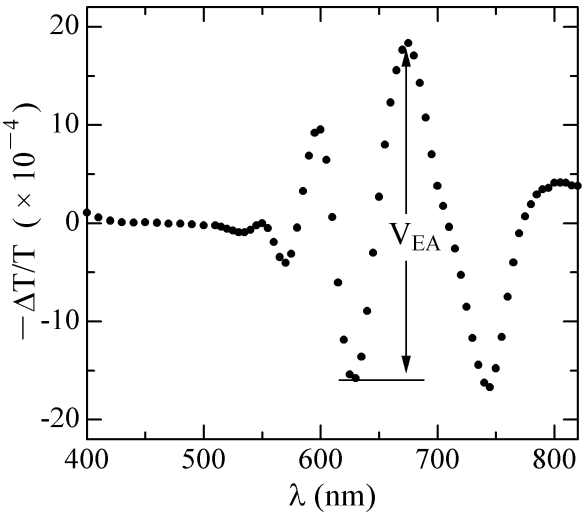

Fig.6 I. Hiromitsu et al.

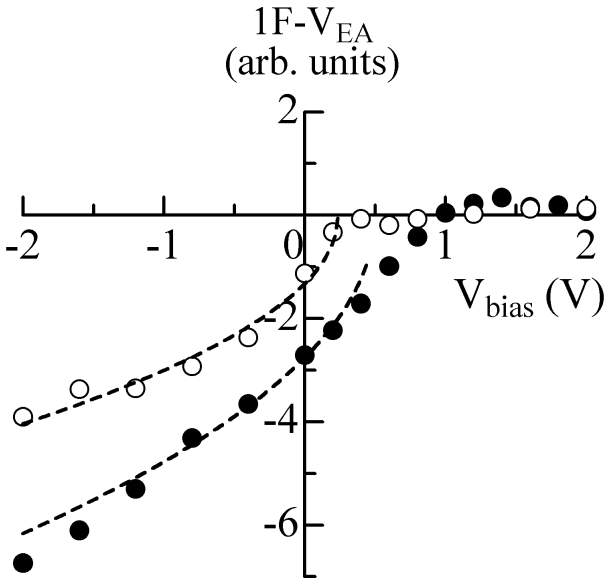

Fig.7 I. Hiromitsu et al.

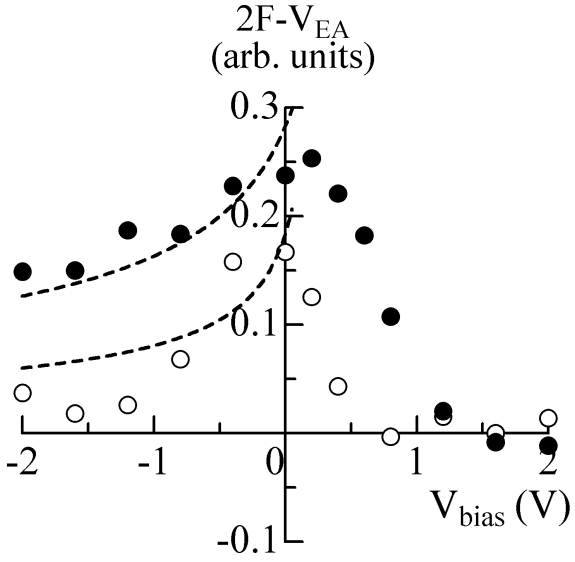

Fig.8 I. Hiromitsu et al.

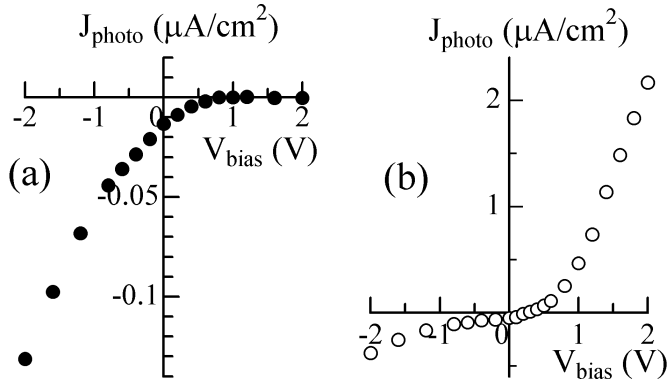

Fig.9 I. Hiromitsu et al.

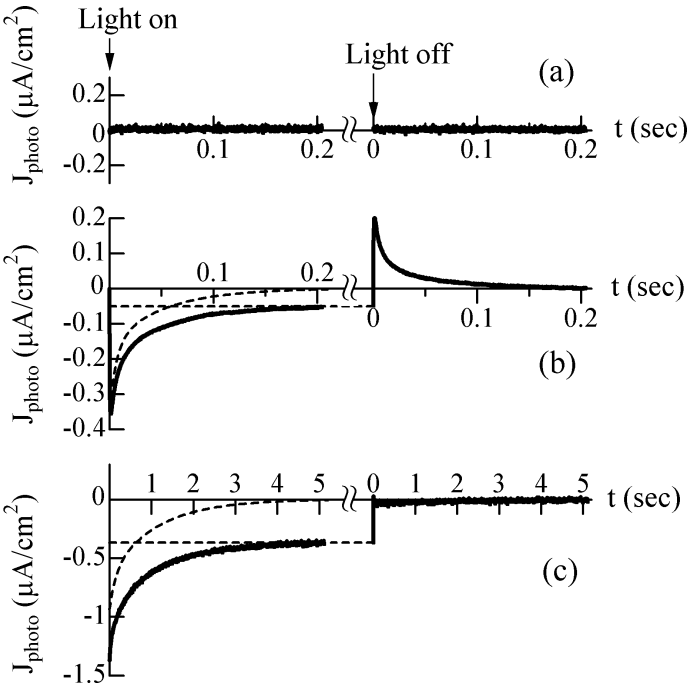

Fig.10 I. Hiromitsu et al.

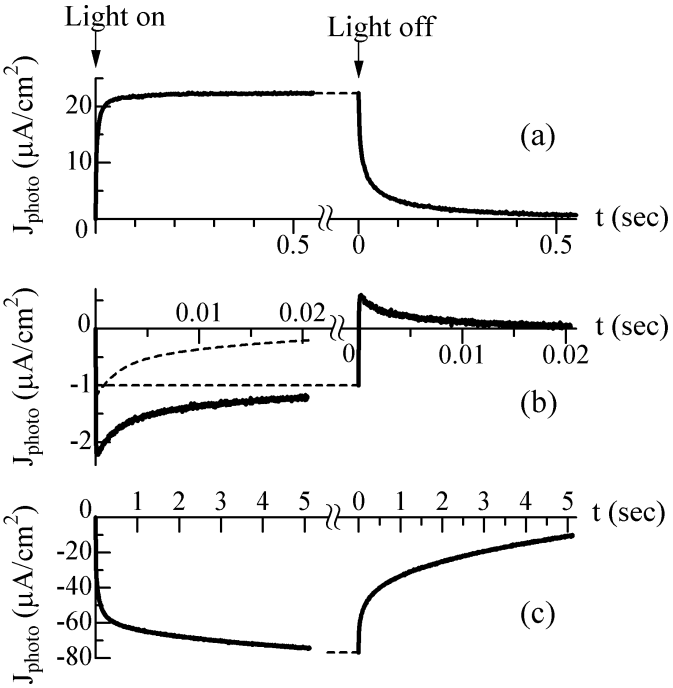

Fig.11 I. Hiromitsu et al.

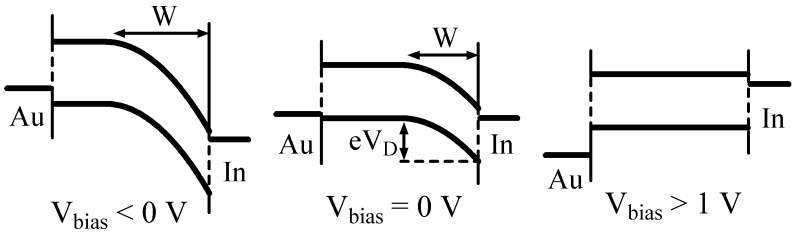

Fig.12 I. Hiromitsu et al.

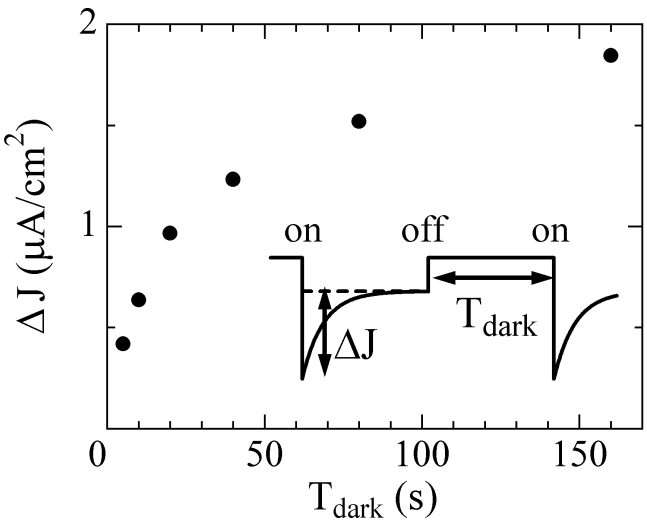

Fig.13 I. Hiromitsu et al.